PERGAMON

International Journal of Heat and Mass Transfer 42 (1999) 4427–4445

International Journal of HEAT and MASS TRANSFER

www.elsevier.com/locate/ijhmt

# Study of double-diffusive velocity during the solidification process using particle image velocimetry

S.Y. Wang, C.X. Lin, M.A. Ebadian*

*Florida International University, Hemispheric Center for Environmental Technology, Center for Engineering and Applied Sciences, 10555 W. Flagler Street, EAS-2100, Miami, FL 33174, USA*

Received 3 August 1998; received in revised form 26 March 1999

**Abstract**

This paper reports the velocity distribution of double-diffusive convection of a binary mixture in a rectangular enclosure during the solidification process. The mixture was a $NH_4Cl$–$H_2O$ solution. The advanced technique, particle image velocimetry (PIV), was used to measure the velocity distribution in the liquid region during solidification. For the purpose of comparison, the solidification of pure water was studied with the same technique. The temperature of the cooling walls in the test chamber and the temperature of the test solution during solidification were also measured. The double-diffusive flow was found to be stronger at the beginning of solidification; the flow decays as solidification proceeds. The velocity distribution of the hypereutectic solution of $NH_4Cl$–$H_2O$ has evident difference in comparison with hypoeutectic solution. 

## 1. Introduction

In recent years, a larger number of experimental and theoretical studies have been devoted to fluid motions associated with the crystallization or solidification process. In particular, it was recognized that double-diffusive heat and mass transfer play important roles due to the coexistence of temperature and concentration gradients in the liquid phase [1,2].

Macrosegregation is an important phenomenon known to occur during the solidification of a mixture. Indeed, it is primarily responsible for the double-diffusive convection during the solidification process. Macrosegregation, the nonuniform macroscope distribution of the components of an alloy during solidification, is a defect that can occur in real metal processing systems. These nonuniformities, especially when they form high compositional gradients, can be areas of high stress concentration, which cause cracking when an aluminum or steel billet is extruded or forged or when an as-cast piece, such as a turbine blade, is severely loaded in service. Although unidirectional solidification has been used to confine the segregation to a small portion of the casting, there is still seriously detrimental convection, driven primarily by thermal and solute density differences. The superalloys are among the alloy systems particularly subject to these effects because of their characteristic lower-density region ahead of the solidification front, where preferential rejection of the lighter species occurs. Since the resultant segregation is density-driven (i.e. a buoyancy effect), it has been suggested that multicomponent materials subject to these phenomena could be processed in the near-zero gravity environment of space to eliminate convective-driven segregation effects.

* Corresponding author. Tel.: +1-305-348-3585; fax: +1-305-348-4176.

*E-mail address:* ebadian@eng.fiu.edu (M.A. Ebadian)

0017-9310/99/$ - see front matter 
PII: S0017-9310(99)00114-3

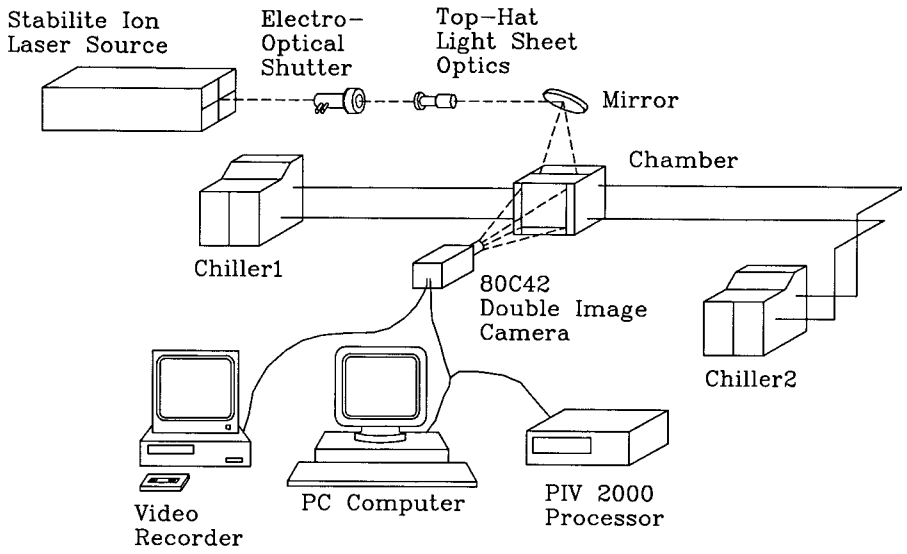


Fig. 1. The PIV velocity measurement system.

Numerous numerical investigations have been conducted to explore the double-diffusive convection flow patterns during the solidification process. Consider the articles of Bennon [3], Beckermann and Viskanta [4], Thompson and Szekely [5], and Oldenburg and Spera [6]. However, few of the numerical results of these investigations have been verified quantitatively by experimental measurements. Measuring velocity using the conventional techniques is difficult because the solidification process is time-dependent and the magnitude of the velocity is small. This is especially true in casting systems. Since liquid metals are opaque, convective flow visualization is almost impossible. Moreover, most molten metals of commercial interest have higher melting temperatures, rendering them difficult to work with in the laboratory under controlled conditions. However, metal model material permits direct optical access into the material, leading to a direct observation of the thermal and concentration fields in real time by classical optical techniques based on a refractive index change of the material. Ammonium chloride ($NH_4Cl$) is a material whose water solution can be used to model metal alloy solidification because it freezes, as does a molten metal of commercial interest. The flow visualization is achievable because a $NH_4Cl$–$H_2O$ solution is transparent.

Several studies have involved flow visualization during the solidification of binary mixtures using $NH_4Cl$–$H_2O$ solution. Asai and Muchi [7] chilled aqueous $NH_4Cl$ solution from both sides in a rectangular enclosure and used a potassium permanganate dye to trace fluid motion in the sidewall mushy region. Under a similar condition, Murakami and Okamoto [8] documented the ejection of crystals or slurry into the melt from the sidewall mushy region. Christenson and Incropera [9] studied the solidification of $NH_4Cl$–$H_2O$ solution in a rectangular cavity with varying initial concentration and thermal boundary conditions. More recently, Magirl and Incropera [10] used a 27% aqueous $NH_4Cl$ solution as a transparent analog medium to observe double-diffusive convective flow in unidirectional solidification by shadowgraph and dye injection techniques. Chen and Chen [11] also studied the unidirectional solidification of aqueous ammonium chloride solution. McCay et al. [12] investigated convective instabilities during directional solidification of $NH_4Cl$–$H_2O$ solution. McCay and McCay [13] studied the solidification of $NH_4Cl$–$H_2O$ solution using a so-called confocal optical processing (COP) technique, which is based on Fourier optics and produces data that are similar to that of an interferometer, but is considerably simpler and more rugged. In addition, Dosch and Beer [14] studied the double-diffusive convection flow using holographic interferometry. All of these studies provided only a qualitative static picture of the convective flow; transient characteristics of the flow were not revealed. In particular, the quantitative picture of flow could not be acquired.

For this paper, particle image velocimetry (PIV), the advanced technique made by DANTEC Measurement Technology, was applied to measure the velocity distribution in the liquid region during the $NH_4Cl$–$H_2O$ solution solidification process. The experiments were conducted in a rectangular enclosure. Two vertical walls and the bottom of the chamber were cooled below the eutectic temperature of the solution and kept constant. The front wall was used for observing. For the purpose of comparison, the solidification of

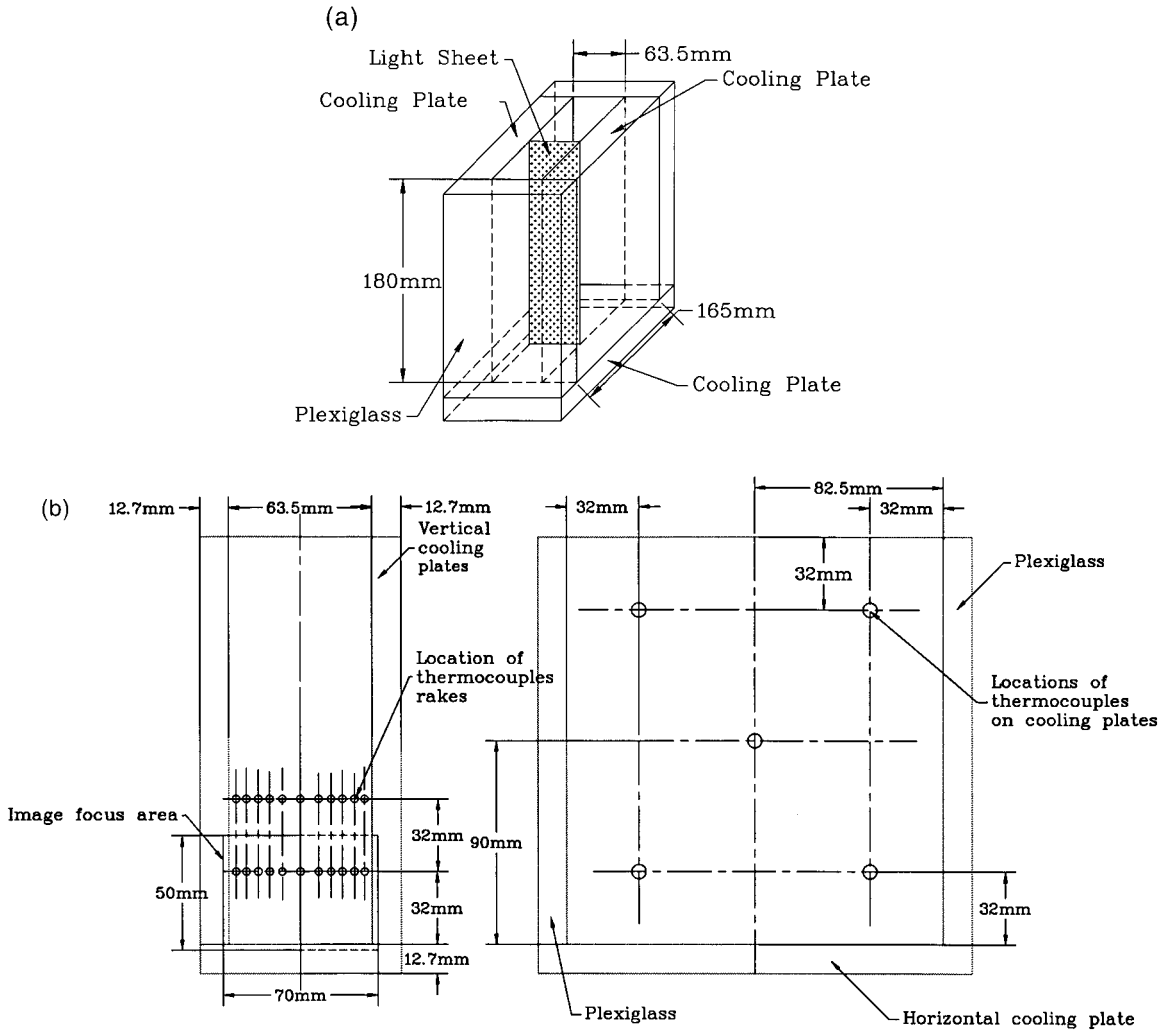


Fig. 2. (a) The test section. (b) The location of thermocouple and image focus areas in test chamber.

pure water was studied with the same technology, and the natural convection induced by temperature gradient was observed. The PIV was set up to track the velocity distribution in the liquid region and the variation with time. In addition, the cooling strength and initial concentration of the mixture were varied to identify the effects of initial concentration and cooling temperatures on the solidification process.

## 2. Experimental system

The schematic of the experimental system is shown in Fig. 1. The test section shown in Fig. 2(a) and (b) is a rectangular enclosure whose inside dimension is 63.5 mm wide, 180 mm high, and 165 mm deep. The 165 mm depth was sufficiently large to render three-dimensional effects negligible. Two vertical cooling walls and the cooling bottom were made of copper plates in which the circulating coolant channels were machined. The rest of the walls were made from 0.5-inch-thick plexiglass. Ten type E copper-constantan thermocouples were well-distributed on the surface of the copper plates to monitor the surface temperature of the vertical walls of the rectangular enclosure, as shown in Fig. 2(b). To prevent corrosion, the surface of the copper plates was protected with a 25-μm-thick Teflon-based coating. The copper cooling plates were chilled with NESLAB HX-540 Recirculating Chiller and NESLAB ULT-90 Recirculating Chiller. One of the chillers initialized the temperature of the solution, and the other one provided the coolant to the test chamber. During the solidification process, a video monitoring system was used to observe the flow

phenomena. Temperature distribution in the test solution was obtained by means of the two horizontal rakes, each of which was installed 20 mm away from the rear plate of the test chamber and contained 11 type E copper-constantan thermocouple junctions. The rakes were positioned at two vertical locations within the test chamber, corresponding to elevations of $y = 32$ mm and 64 mm from the bottom of the chamber as shown in Fig. 2(b). The spacing between thermocouple junctions was staggered, with more junctions installed near the cold walls where large temperature gradients were expected. The output voltages of the thermocouples were measured using a LabVIEW data acquisition system, which was controlled by a graphical program written with LabVIEW software and run on a personal computer. The standard limit of uncertainty of type E thermocouples is $\pm 1.7^{\circ}C$, while the reference junctions in the multiplexes have an uncertainty of $\pm 0.3^{\circ}C$.

PIV from DANTEC was used to obtain the velocity-vector plots containing both velocity amplitude and flow direction for the whole-visualized flow field with high accuracy and high resolution. Basically, a PIV system includes four main subsystems: visualization, photographs (cameras), video recordings, and analysis software. A laser is the ideal light source for PIV illumination because of its high intensity, directionality, and easier optical control. For low-speed flows, where only a small area of the flow field is of interest, a shutter-grated, continuous wave laser is used. In our illumination system, the Stabilite® 2017 Ion Laser was used as a continuous wave (CW) laser. The beam from the CW laser was chopped into pulses by DANTEC's $80 \times 41$ Electro-Optical Shutter. As with the pulsed laser illumination method, the chopped beam was then expanded by a lens system (e.g. the $80 \times 40$ Top-Hat Light-Sheet Optics) to form a pulsing light sheet.

DANTEC's 80C42 DOUBLEImage 700 Camera was used to record images of an illuminated section. The 80C42 DOUBLEImage 700 Camera contains a video format CCD chip and special electronics for fast interframe acquisition of two images. The CCD chip was exposed to scattered light from the first pulse of the light sheet, and the $768 \times 484$ pixel image was acquired. The CCD chip was then cleared and exposed to scattered light from the second pulse of the light sheet, and a second full $768 \times 484$ pixel image was acquired. Both images were then transferred to DANTEC's PIV 2000 Processor via the digital connector and host computer for data processing and analysis, and the images recorded by the camera were transferred to a video recorder to show flow pattern in the same time.

The 80C42 DOUBLEImage 700 Camera may work in three different modes: (1) double-frame, cross-correlation mode; (2) single-frame, cross-correlation mode; and (3) single-frame, auto-correlation mode. By far, the most powerful operating mode with the 80C42 DOUBLEImage 700 Camera is the double-frame cross-correlation. In this mode, one can use cross-correlation to obtain a vector without directional ambiguity with pulse separations anywhere from 66 ms down to 2 μs, allowing measurement of very low up to supersonic speeds. The PIV 2000 Processor is a core part of DANTEC's PIV system and has a modular structure. There are three units that can be inserted into the processor: a correlator unit, input buffers, and a synchronization unit.

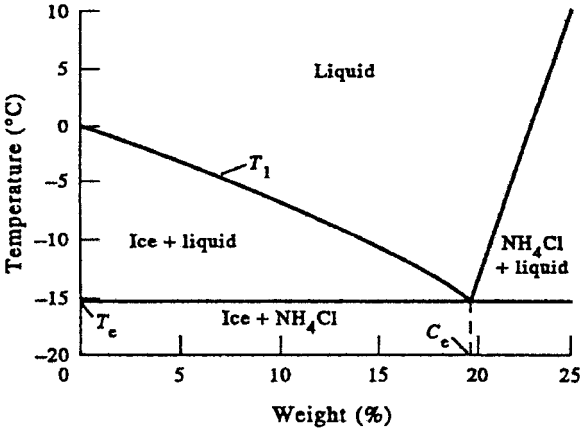


Fig. 3. Equilibrium phase diagram for $NH_4Cl$–$H_2O$ [20].

In PIV, it is not actually the velocity of the flow that is measured, but the velocity of particles suspended in the flow. In this respect, these seeding particles can be considered as probes, and seeding considerations are thus important in PIV. The particles must be small enough to track the flow accurately, yet large enough to scatter sufficient light for the camera to be able to detect them. Ideally, the particles should also be neutrally buoyant in the fluid; that is, they should have approximately the same density as the fluid itself. Strictly speaking, utilizing particles in double-diffusive convection is limited due to the low velocity involved and the density variations present in the fluid. Care should therefore be taken when choosing particles to visualize the convection flow. During the 1970s, using particles to visualize flow field in the double-diffusive convection they had reported, Chen et al. [15] used aluminum particles to visualize flow in the developed layers formed by heating a stable salinity gradient from a side wall. Huppert and Linden [16] used aluminum particles to observe the structure of flow in a stable solute gradient heated uniformly from below. Silvered hollow particles made by POTTERS Industries, Inc., that have almost the same density as the solution served as the seeding in this study. The di-

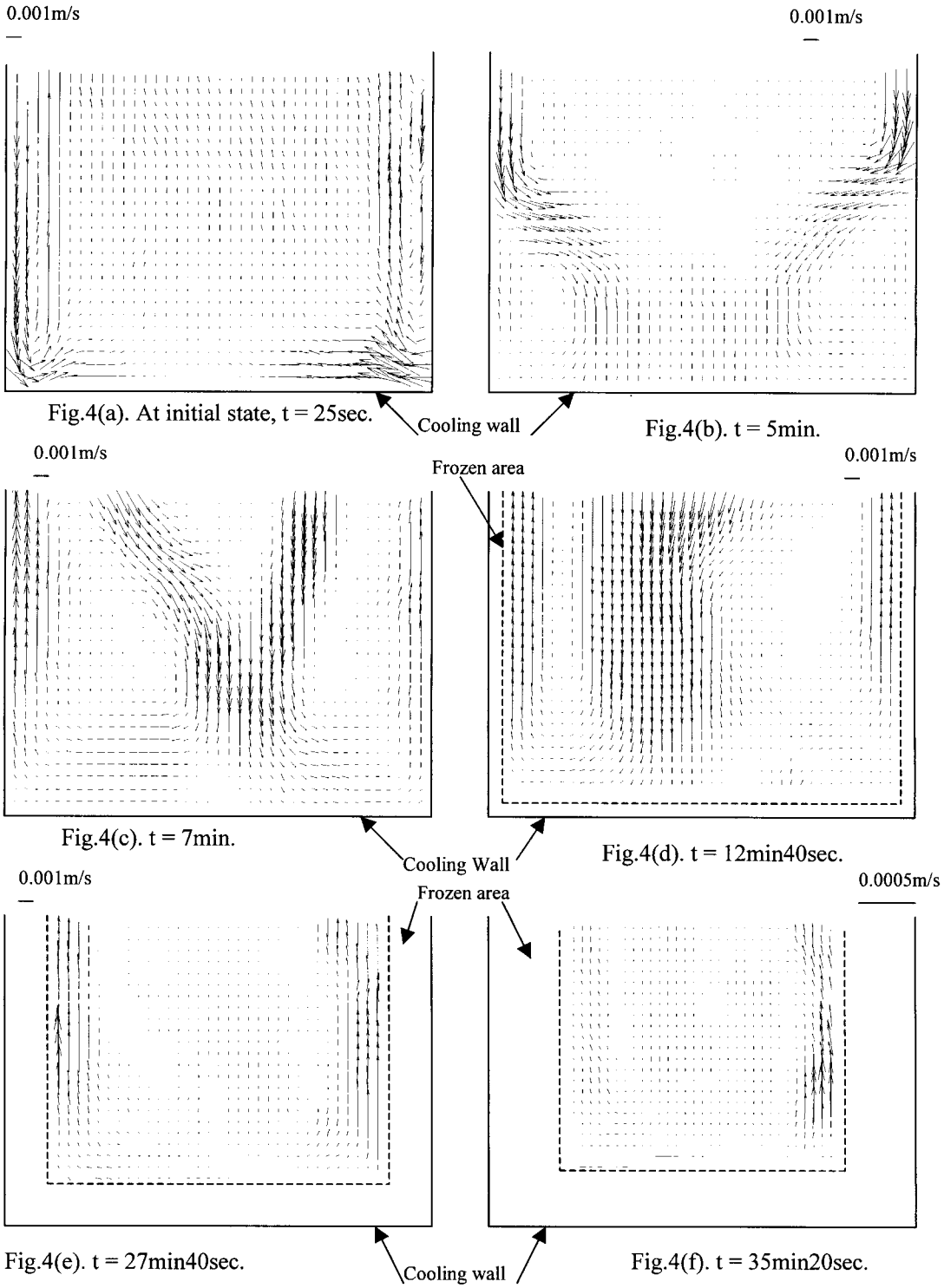


Fig. 4. The velocity vectors of pure water solidification.

Table 1
Experimental test parameters

| Case no. | Initial concentration of solution (wt%) | Density ($kg/m^3$) | Initial temperature of solution (°C) | Output coolant temperature (°C) | Time between pulses (μs) | Duration of each pulse (μs) | Time between recording (ms) | Light pulses per recording |
|---|---|---|---|---|---|---|---|---|
| 1 | Pure water | 1000.0 | 23 | −8 | 60 000 | 3000 | 20 000 | 2 |
| 2 | 10 | 1046.0 | 23 | −36 | 60 000 | 3000 | 20 000 | 2 |
| 3 | 10 | 1046.0 | 23 | −25 | 60 000 | 3000 | 20 000 | 2 |
| 4 | 15 | 1056.6 | 23 | −25 | 60 000 | 3000 | 20 000 | 2 |
| 5 | 22 | 1061.0 | 23 | −40 | 60 000 | 3000 | 20 000 | 2 |

ameter of a silvered hollow particle is 10 μm. Both water and $NH_4Cl$–$H_2O$ solution were used for solidification. The $NH_4Cl$–$H_2O$ solution was held at the eutectic concentration of 19.7%, and the eutectic temperature is −15.4°C. The equilibrium phase diagram for aqueous ammonium chloride is shown in Fig. 3. This solution was selected for several reasons: (1) its semitransparency, which facilitates flow visualization; (2) its similarity to liquid metal solidification in term of dendritic growth of the solid phase; (3) the availability of thermophysical property data, which facilitates numerical simulation; and (4) the flexibility that it provides for experimenting magnitude and direction. A major disadvantage of $NH_4Cl$–$H_2O$ solution is its extreme corrosiveness, which significantly reduces the life of test cell components and instrumentation.

As mentioned above, in our illumination system, the Stabilite® 2017 Ion Laser was used as a continuous wave (CW) laser; DANTEC's 80C42 DOUBLEImage 700 Camera was used to record images of an illuminated section, but only a small area of the test chamber can be detected by the camera of the PIV system. The obtained image area or image focus area was 50 × 70 mm, as shown in Fig. 2(b). The detected area, near the bottom of the test chamber, included the two vertical cooling plates and the bottom cooling plate.

## 3. Results and discussion

To begin the experiment, a solution of desired composition was prepared by mixing the corresponding amount of ammonium chloride and water. After the solution was poured into the chamber, the chiller established the initial temperature of the solution. The depth of the solution in the chamber was 160–170 mm, liquid surface exposed in the atmosphere. After the initial temperature of the solution was established, the coolant with the constant temperature was connected to the test chamber to begin the solidification process.

### 3.1. Pure water

The pure water solidification process was measured by PIV in the first try. A set of pictures of the pure water velocity vector during solidification was measured with PIV, as Fig. 4 shows. The test parameters are shown in Table 1. Double-frame, cross-correlation mode was used. The interrogation areas were 32 × 32 pixels. Overlap was horizontal: 50%, vertical: 50%. The water near the vertical cooling walls flowed downward along the vertical cooling walls, and there was upward flow of greater velocity close to the downward flow layer. The water in the middle of the test chamber flowed upward, and the water close to

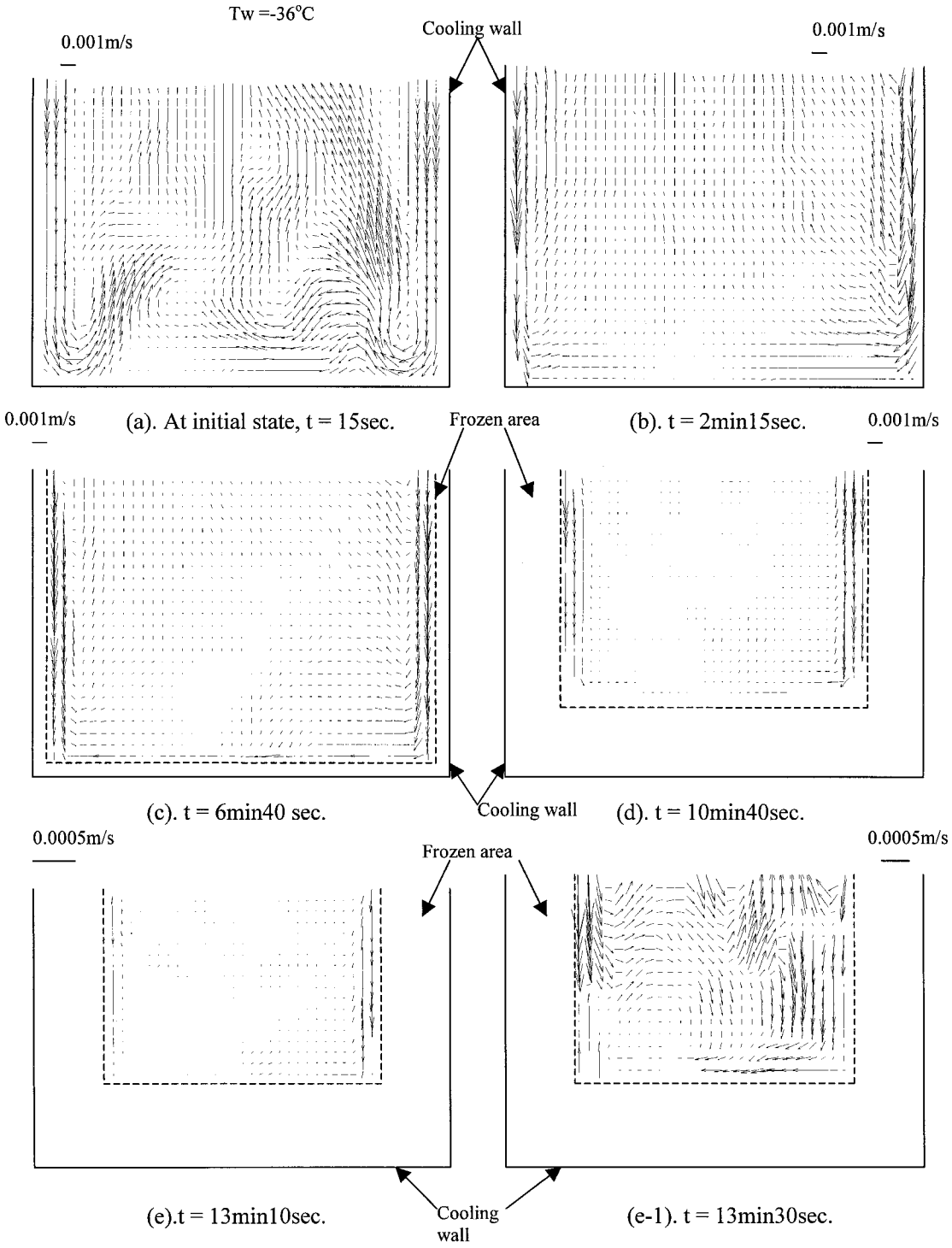


Fig. 5. The velocity vectors of 10wt% $NH_4Cl$–$H_2O$ solution solidification.

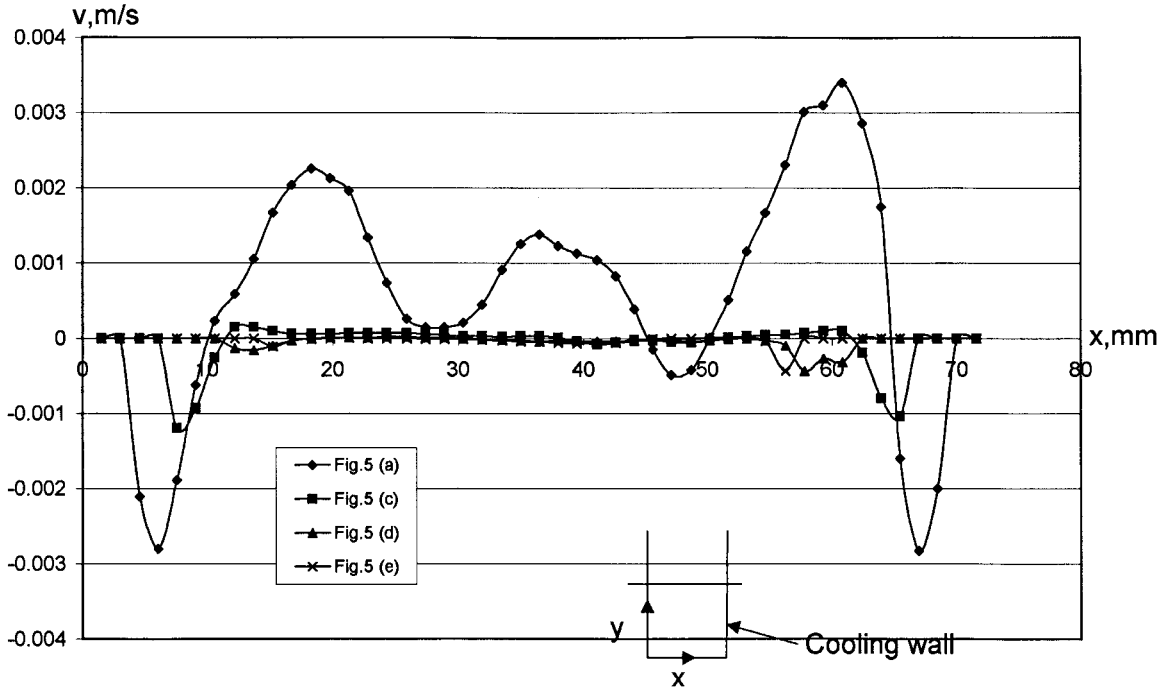


Fig. 6. Comparison of the $y$-direction velocity component at different times from a lateral cut of velocity vector drawings in Fig. 5 at $y = 23.5$ mm.

the bottom cooling wall flowed from both sides to the middle, as in Fig. 4(a).

During the first 5 min, the cooling walls had cooled the water. The temperature of the water reduced continuously. When the temperature of the water was reduced to 4°C, the density of the water was at maximum. This water flowed along the vertical cooling walls and accumulated near the corners of the chamber. Because its density was maximum, the follow flowed water could not push it and only separated from the cooling walls near the corners of the chamber and flowed toward the middle of the chamber. At the same time, the water accumulated at the corners of the chamber was cooled continuously, the temperature reduced further and the density of the water smaller than that at 4°C. However, the water flowed toward the middle of the chamber had greater density than that accumulated at the corners of the chamber. This greater density water pushed the water at the corners along the bottom and vertical cooling walls to form the vortex flow at the left and right corners of the chamber [17], as shown in Fig. 4(b). The two vortex flows progressed upward close to the cooling walls near the corners of the chamber, and the downward water flow along the left and right cooling surfaces separated from those surfaces. After 7 min, as Fig. 4(c) shows, the former downward flow along the cooling surfaces had changed direction, but the former vortex flow was retained. After 12 min 40 s, ice was observed on the cooling walls, as shown in Fig. 4(d). The figure shows that the main flow along the left and right cooling surfaces had completely changed to flow upward. The vortex flow at the left corner had completely disappeared, and the bulk flow in the middle of the chamber flowed downward. After 27 min 40 s, the ice thickness had obviously increased, and the bulk flow was very weak, except for an upward flow close to the left and right frozen surfaces of the chamber, as Fig. 4(e) shows. After 35 min 20 s, as shown in Fig. 4(f), the flow in the chamber was almost static, except the small quantity of water that flowed upward along the frozen surfaces was flowing at a lower velocity.

### 3.2. $NH_4Cl$–$H_2O$ solution

The double-diffusive convection flow of the solidification of the $NH_4Cl$–$H_2O$ solution was also measured using PIV. Double-frame, cross-correlation mode was used. The interrogation areas were $32 \times 32$ pixels. Overlaps were horizontal: 50%, vertical: 50%. A set of the flow velocity vector drawings of 10 wt% $NH_4Cl$–$H_2O$ solution during solidification process is shown in Fig. 5. The temperature of output coolant in the chiller was set at $-36$°C. The test parameters are shown in Table 1, Case 2. Fig. 5(a) shows that at the beginning of the test, the liquid close to the left and right cooling

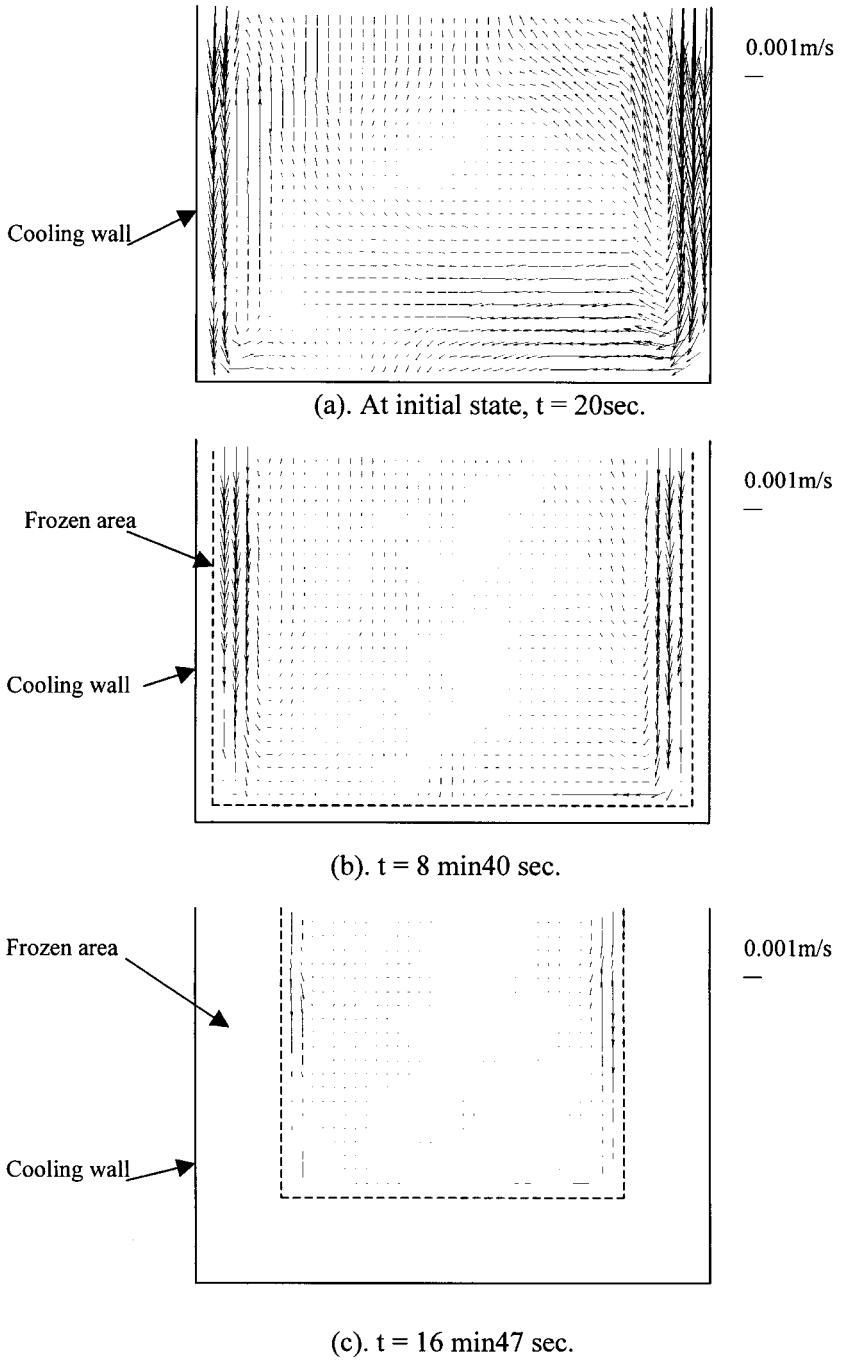


Fig. 7. The velocity vectors of 10 wt% $NH_4Cl$–$H_2O$ solution solidification. $T_w = -25°C$.

walls flowed downward with a greater velocity because it was directly cooled by the left and right cooling walls.

There was a larger temperature gradient in the test solution near the cooling walls. There was also an upward flow at a greater velocity close to the downward flow. The flow in the middle of the chamber was upward. After 2 min 15 s, Fig. 5(b), the flow velocity along the vertical cooling walls became slow because the temperature gradient in the solution near the cooling walls had decreased, but freeze did not begin. After 6 min 40 s, as shown in Fig. 5(c), the solidification of

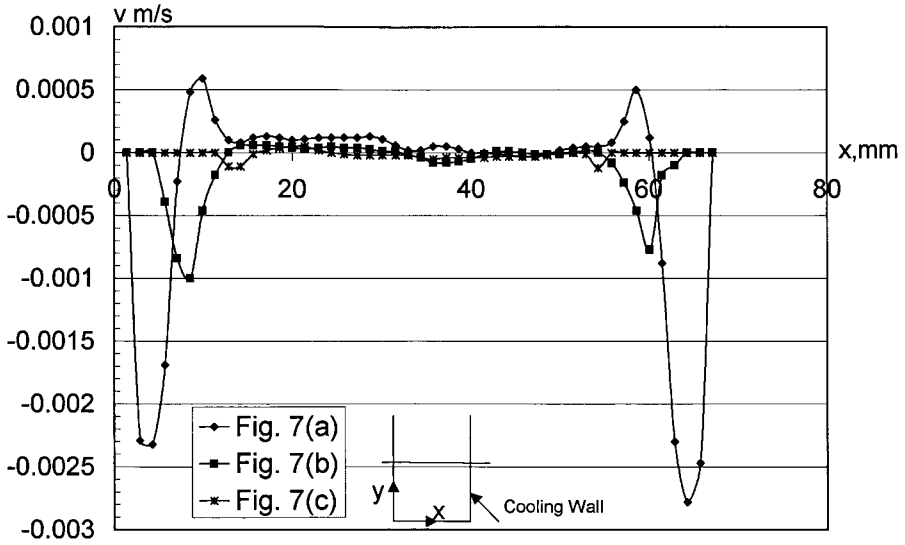


Fig. 8. Comparison of the $y$-direction velocity component at different times from a lateral cut of velocity vector drawings in Fig. 7 at $y = 23.5$ mm.

the $NH_4Cl$–$H_2O$ solution was observed. Because the solidification of the $NH_4Cl$–$H_2O$ solution with a concentration of 10% by weight is hypoeutectic crystallization, the solute-rich liquid was rejected from the interdendritic region. It has a higher density with the bulk liquid, so the solutal buoyancy force enhanced the thermal buoyancy force, and the liquid close to the left and right frozen surfaces flowed downward continuously.

Although the solutal buoyancy force enhanced the thermal buoyancy force, it was greatly reduced for two reasons. First, the convection heat transferred continuously, and second, latent heat of crystallization was released. The flow velocity downward along the vertical frozen surfaces was not faster than before freeze began. The flow in the middle region of the chamber was upward. As shown in Fig. 5(d), with the solidification of the $NH_4Cl$–$H_2O$ solution, the frozen thickness on the left and right cooling wall surfaces continued to increase, and the liquid along the frozen surfaces flowed downward continuously, but the flow velocity was lower than before because the convective heat transfer became conductive gradually, and a lot of small dendrites that obstructed liquid flow along the frozen surfaces had formed.

After 13 min 10 s, the flow of liquid along the frozen surfaces had become very weak, and the bulk liquid flow in the middle region of the chamber had almost stopped, as Fig. 5(e) shows. The extreme slow flow in the liquid area of the chamber could not be detected by using the double-frame, cross-correlation mode. By using single-frame, cross-correlation mode, the flow pattern could still be detected (see Fig. 5(e-1)). Fig. 6 shows the quantitative comparison of y-direction component of the velocity at the different time—obtained by laterally cutting each of the velocity vector drawings in Fig. 5 [except Fig. 5(b)] at the cross-section location of $y = 23.5$ mm from the bottom cooling wall.

The other set of flow velocity vector drawings of 10 wt% $NH_4Cl$–$H_2O$ solution during the solidification process is shown in Fig. 7. The temperature of output coolant in the chiller was set at $-25^{\circ}C$. The other parameters are shown in Table 1, Case 3. From Case 3 in the table, it is obvious that the flow pattern of the solution solidification process was fundamentally the same as the one shown in Fig. 5. Only the freezing speed was lower. Fig. 8 shows the quantitative comparison of the $y$-direction velocity component, also obtained by making a lateral cut at $y = 23.5$ mm for each of the drawings in Fig. 7.

The flow velocity vector drawings of 15 wt% $NH_4Cl$–$H_2O$ solution during the solidification process appear in Fig. 9. The temperature of output coolant in the chiller was set at $-25^{\circ}C$. The other parameters are shown in Table 1, Case 4. From Case 4 it is clear that the flow pattern of the solution solidification process was fundamentally the same as the one shown in Fig. 7. Only the freezing speed is different. As shown in Fig. 9(b) and Fig. 7(b), in order to form the same frozen thickness, it took 5 min 40 s for the 15 wt% $NH_4Cl$–$H_2O$ solution, and it took 8 min 40 s for the 10 wt% $NH_4Cl$–$H_2O$ solution, at the same temperature of output coolant of chiller $-25^{\circ}C$. Fig. 10 shows the quantitative comparison of the $y$-direction velocity component also obtained by making a lateral cut at $y = 23.5$ mm for each of the drawings in Fig. 9.

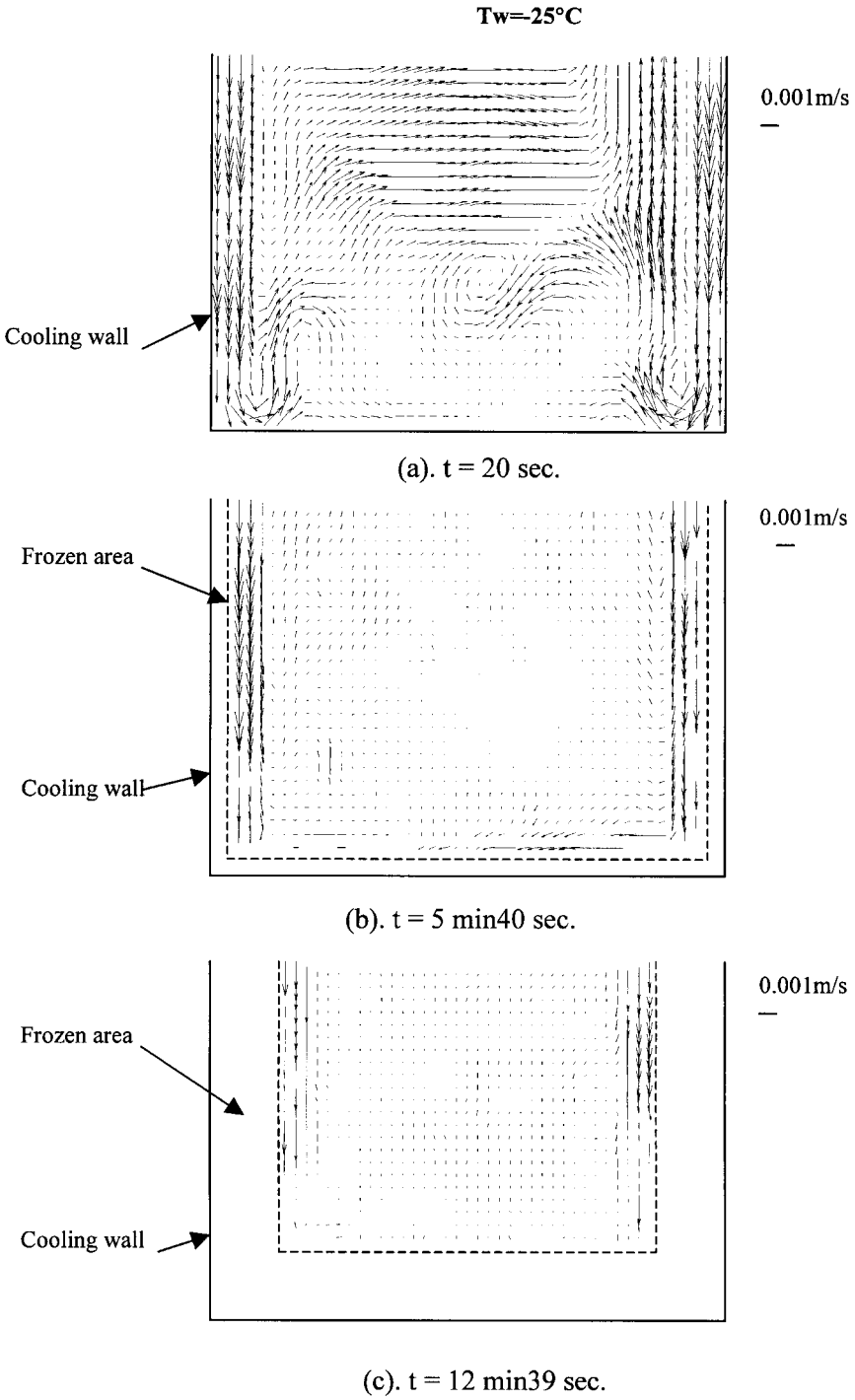


Fig. 9. The velocity vectors of 15 wt% $NH_4Cl$–$H_2O$ solution solidification. $T_w = -25°C$.

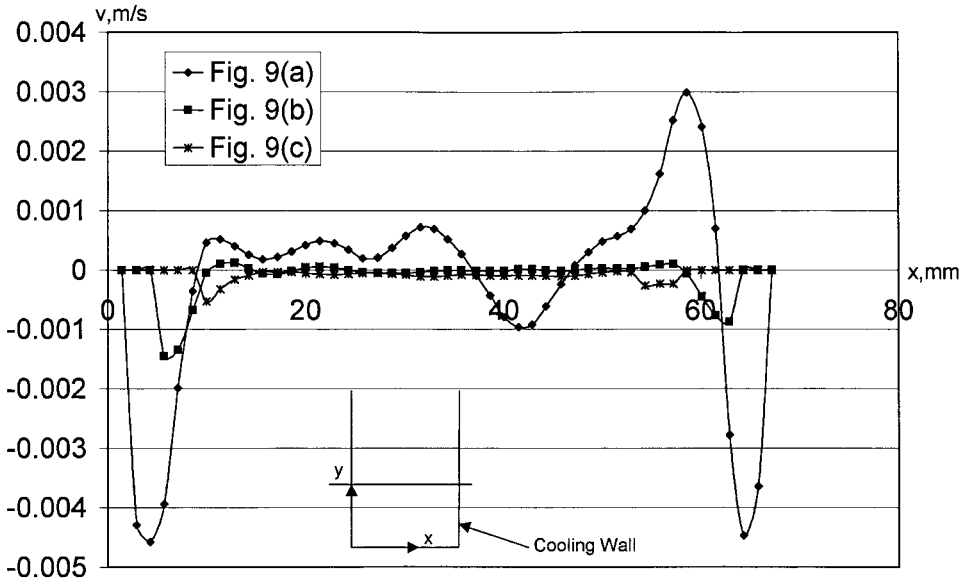


Fig. 10. Comparison of the $y$-direction velocity component at different times from a lateral cut of velocity vector drawings in Fig. 9 at $y = 23.5$ mm.

Fig. 11 shows the comparison of the velocity of double-diffusive convection for different concentrations of $NH_4Cl$–$H_2O$ solutions during the solidification process at the same frozen thickness, with the same output coolant temperature of chiller, when level cross-cutting the relative velocity vector drawings at $y = 23.5$ mm away from the bottom cooling wall. It was obvious that the velocity of 15 wt% $NH_4Cl$–$H_2O$ solution was greater than the 10 wt% $NH_4Cl$–$H_2O$ solution, especially during the early stage of solidification. Here the frozen thickness obtained from the velocity vector drawings related to the solidification process. The real frozen thickness can be obtained by multiplying the above thickness by the object: image scale factor.

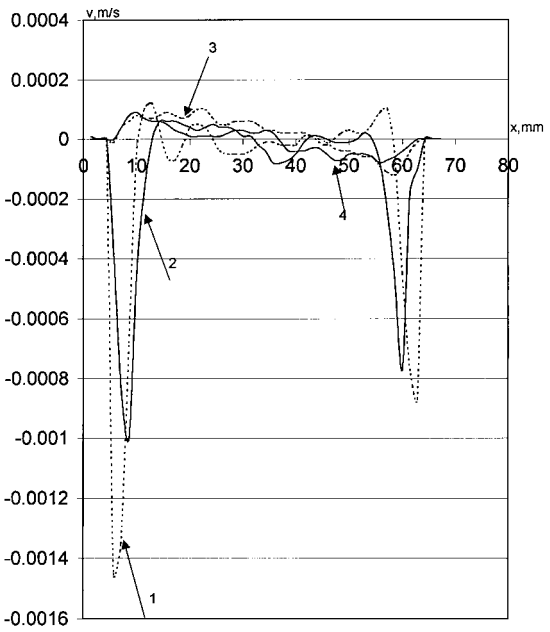


Fig. 11. Comparison of the velocity for different concentration $NH_4Cl$–$H_2O$ solutions at same frozen thickness, same coolant temperature. 1—$v$ vs $x$, 15wt%; 2—$v$ vs $x$, 10wt%; 3—$u$ vs $x$, 15wt%; 4—$u$ vs $x$, 10wt%. $T_w = -25°C$, $h = 1.45$ mm. Comparing Fig. 7(b) with Fig. 9(b).

Fig. 12 shows the comparison of the velocity of double-diffusive convection of $NH_4Cl$–$H_2O$ solution during the solidification process for different output coolant temperatures at the same frozen thickness, the same solution concentration, and when level cross-cutting the relative velocity vector drawings at $y = 23.5$ mm away from the bottom cooling wall. Fig. 12 shows the velocity at temperature of $-36°C$ of output coolant was greater than at $-25°C$, when the frozen thickness on the cooling walls was 1.45 mm. When the frozen thickness increased, the velocity difference between the two cases decreased.

A set of the flow velocity vector drawings of 22 wt% $NH_4Cl$–$H_2O$ solution during the solidification process is shown in Fig. 15. The temperature of the test solution during the solidification process was also measured using thermocouples as shown in Figs. 13 and 14. The other parameters are shown in Table 1, Case 5. Fig. 15(a). The output coolant temperature of the chiller was set at $-40°C$. The temperature of the two vertical cooling walls was measured using thermocouples as shown in Fig. 16 shows that at the begin-

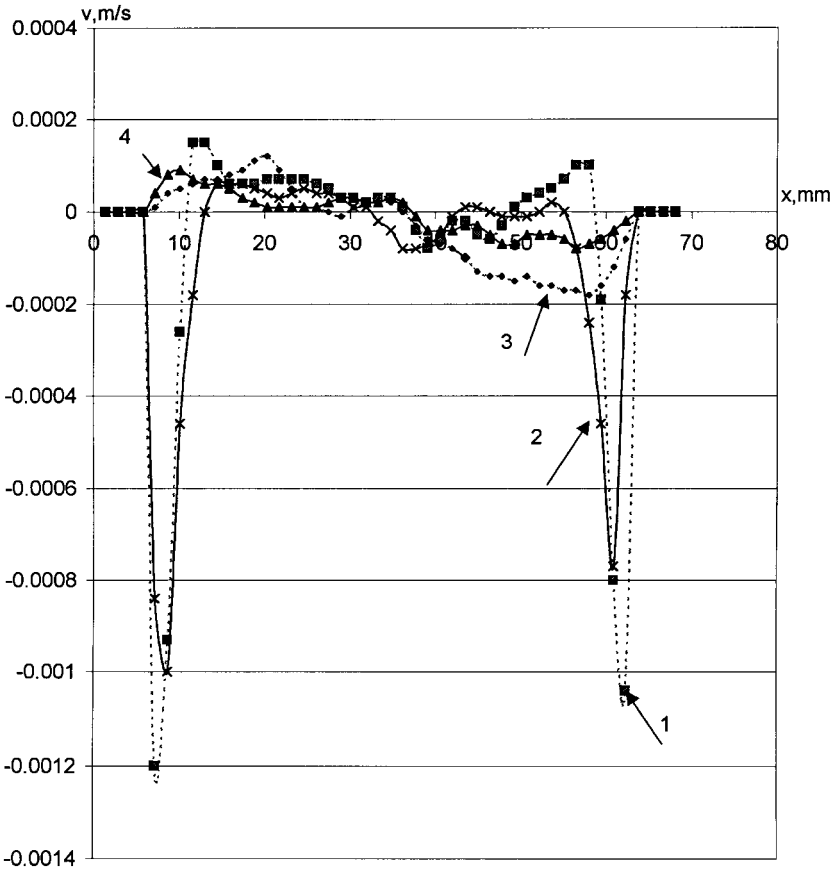


Fig. 12. Comparison of the velocity for different output coolant temperatures at same concentration, same frozen thickness. 1—$v$ vs $x$, $T_w = -36°C$; 2—$v$ vs $x$, $T_w = -25°C$; 3—$u$ vs $x$, $T_w = -36°C$; 4—$u$ vs $x$, $T_w = -25°C$. $C$ = 10wt%, $h$ = 1.45 mm. Comparing Fig. 5(c) with Fig. 7(b).

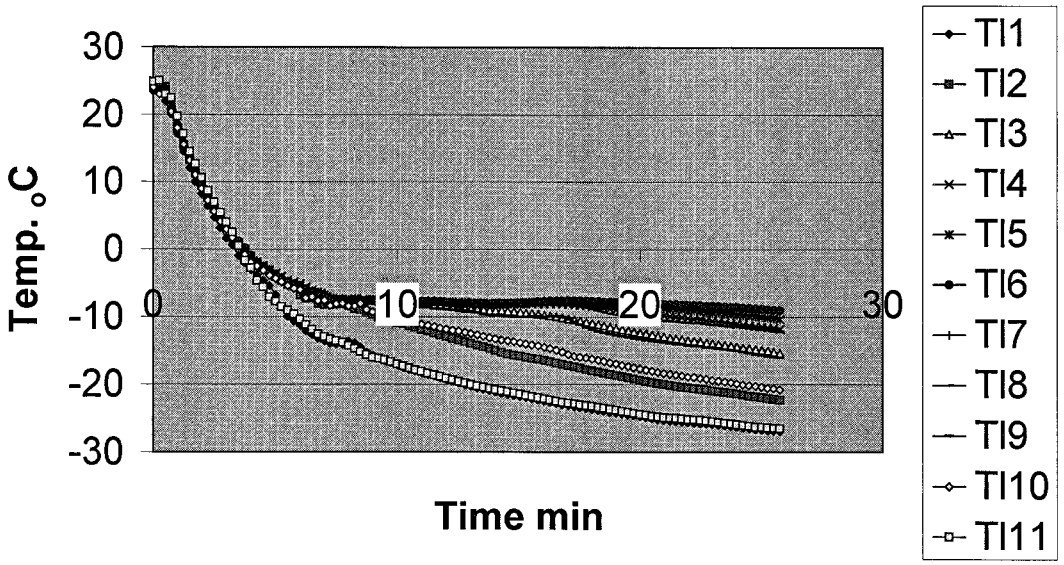


Fig. 13. Temperature of 22 wt% $NH_4Cl$–$H_2O$ solution during solidification (1).

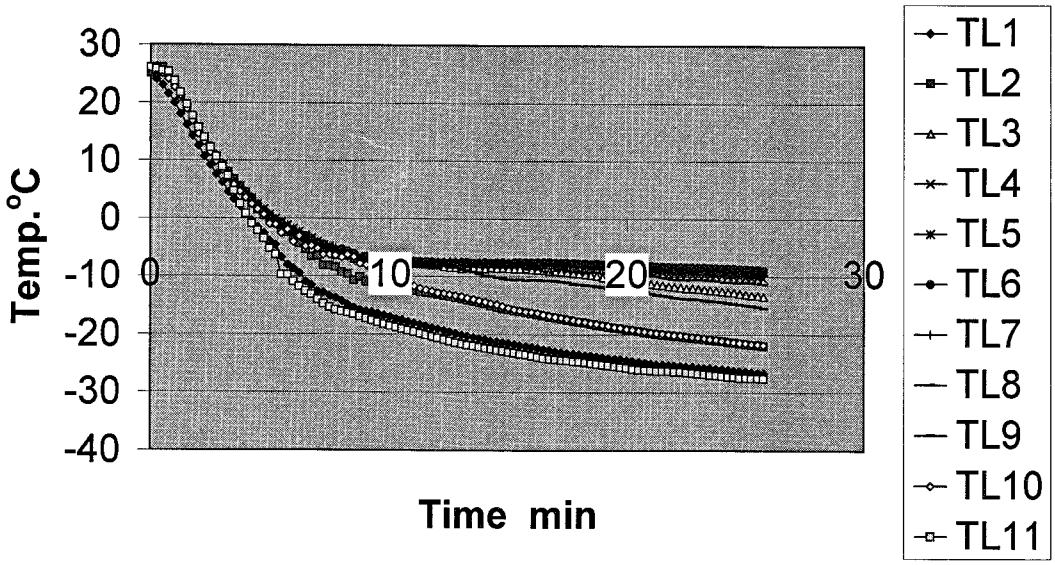


Fig. 14. Temperature of 22 wt% $NH_4Cl$–$H_2O$ solution during solidification (2).

ning of the test, the liquid close to the left and right cooling walls flowed downward with a greater velocity, as happens with pure water, and hypoeutectic solidification process because it was directly cooled by cooling walls. There was also an upward flow at a greater velocity close to the downward flow. After 3 min 4 s, as Fig. 15(b-1) shows, the frozen thickness on cooling walls in the chamber can be seen; that is, the solidification of 22 wt% $NH_4Cl$–$H_2O$ solution had evidently begun. Because the solidification of $NH_4Cl$–$H_2O$ solution with a concentration of 22% by weight is hypereutectic crystallized, the water-rich liquid was rejected from the interdendritic region. Its lower density, with respect to the bulk liquid, caused it to ascend. This upward flow affected the downward thermal flow that existed along the frozen solids interface and contributed to the turbulent regime that was present. Yet there was still a large enough temperature gradient near the frozen solids interface; the liquid close to the left and right frozen surfaces flowed downward continuously, as Fig. 15(b) shows. In this hypereutectic case, the solid matrix in the mush zone consists of crystallized ammonium chloride. Crystallization of ammonium chloride yields a structurally 'fragile' matrix [18]. As shown in Fig. 15(b-1), $NH_4Cl$ crystals 'break off' at the solid/mush interface and after they are carried by the fluid or they fall down by gravity, they settle at the vicinity of the bottom of the chamber, especially the corner of the test chamber. In addition, such crystals are created in the undercooled liquid phase, away from the mush zone [18]. As $NH_4Cl$ crystals or dendrites break off, they would be seen as seeding particles as flow field tracers. These particles seeding together with seeding particles especially added to the test solution before the test start were captured by the camera in the PIV system and yielded the image of flow field and velocity vector drawings as shown in Fig. 15(b). There were a lot of velocity vectors near the velocity vector of flow downward along the frozen surfaces. They actually were velocity vectors of the broken-off crystals or dendrites, as shown in Fig. 15(b-1). After 10 min 28 s, as shown in Fig. 15(c) and (c-1), a large number of the crystals or dendrites had heaped on the bottom of the chamber, particularly at the corners so that no velocity vector of liquid could be obtained at the area of heaped crystals. It is not significant to study the velocity of the flow field continuously at the image focus area. The main study concentrated on a high area in the test chamber, as shown in Fig. 2(b), that is, a higher image focus area. Because so many broken-off crystals or dendrites added to the bulk liquid in the test chamber, the bulk liquid did not present a pure liquid phase. It became a mixed phase, that is, liquid (bulk liquid) and solid (broken-off crystal or dendrite). Liquid and solid acted upon each other. The pattern of flow field of the liquid region in the chamber became more complex.

The test was to be done under the same conditions with former 22 wt% $NH_4Cl$–$H_2O$ solution. Only the image focus area was higher than before. At 2 min 15 s after the test started, as shown in Fig. 15(d), the solidification of the $NH_4Cl$–$H_2O$ solution began. The liquid along the frozen surface flowed downward; the liquid in the middle of the chamber flowed upward slowly.

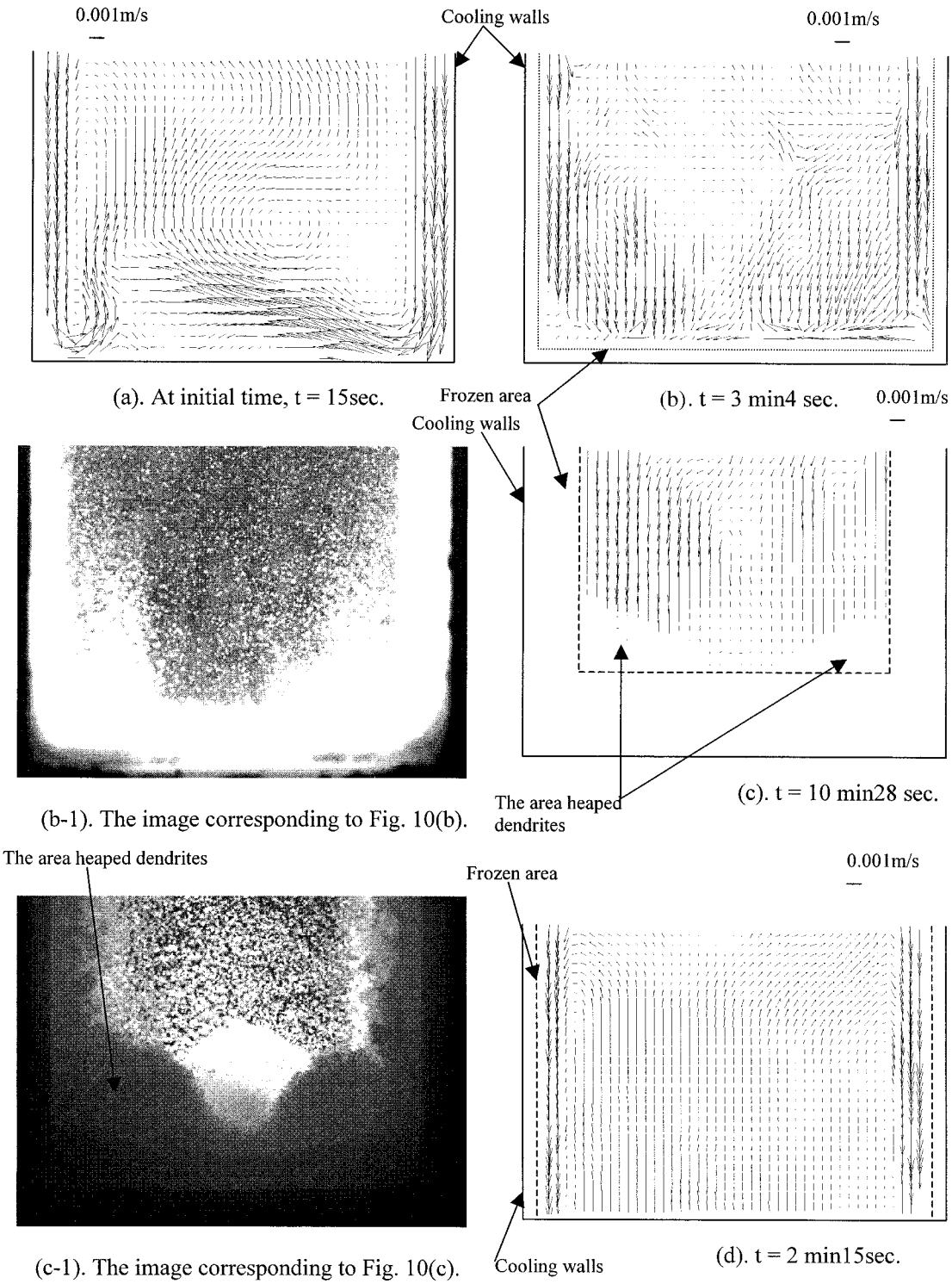


Fig. 15. Velocity vectors of 22 wt% $NH_4Cl$–$H_2O$ solution solidification.

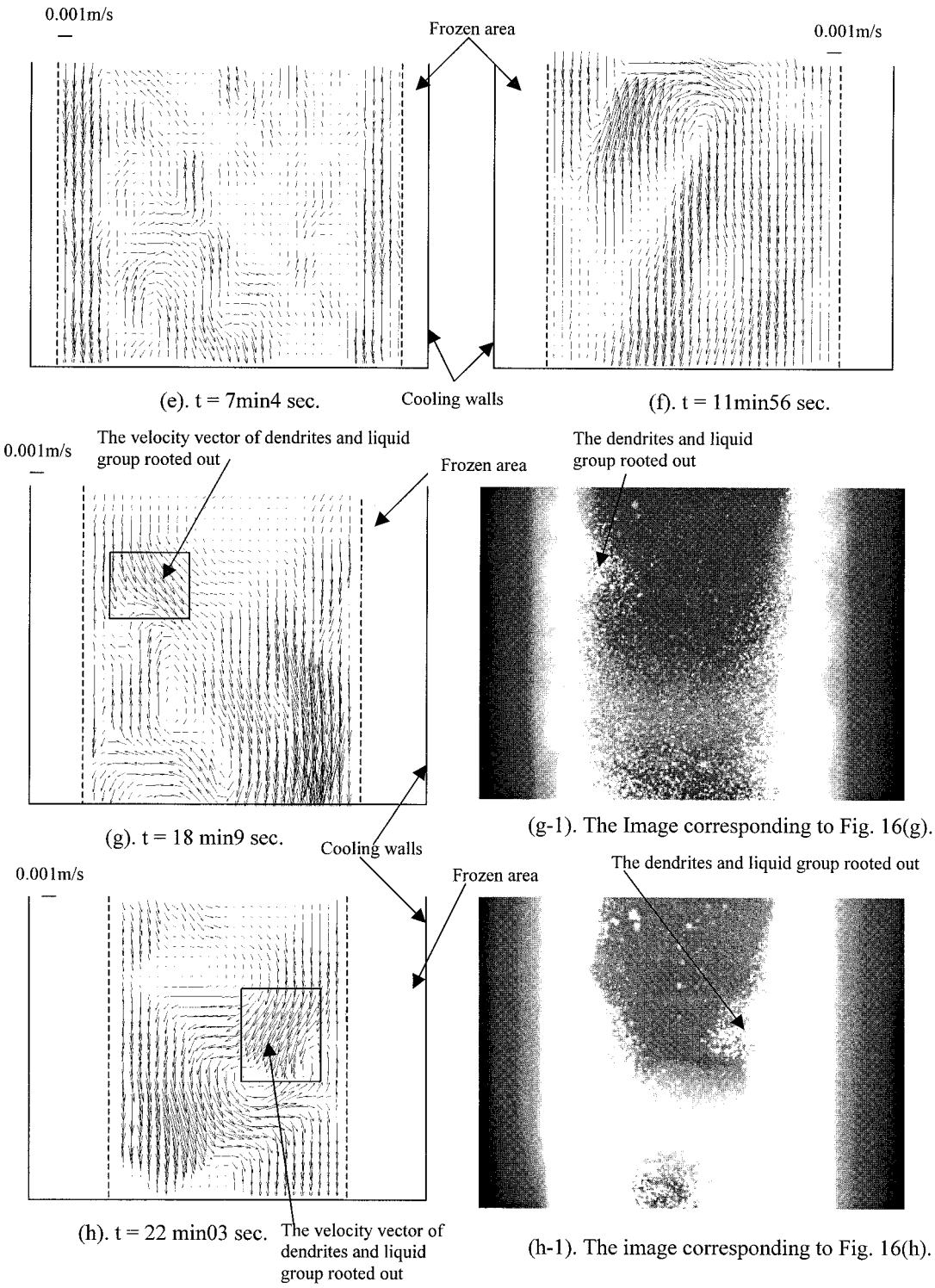


Fig. 15 (*continued*)

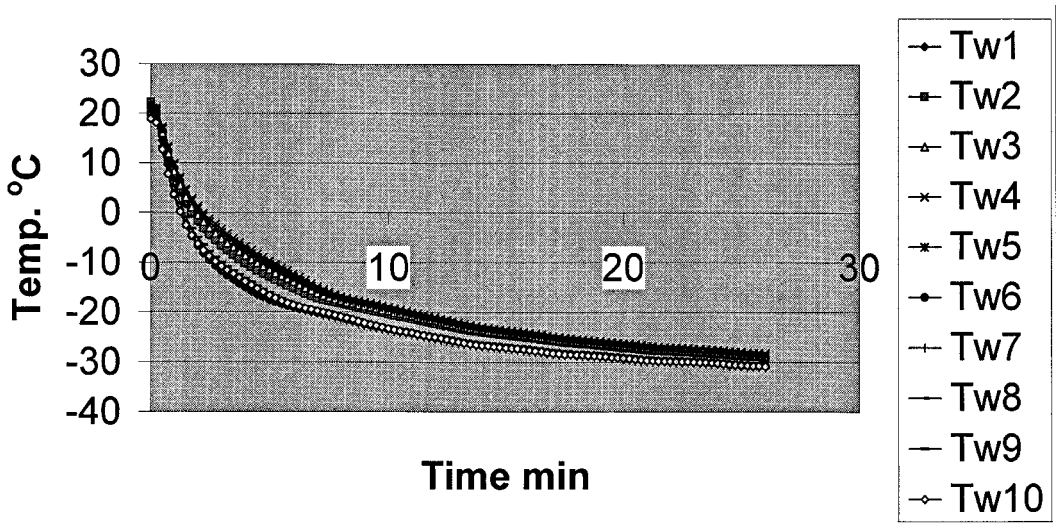


Fig. 16. Temperature of cooling walls during solidification of 22 wt% $NH_4Cl$–$H_2O$ solution.

At this moment, the liquid zone in the chamber can be considered a pure liquid phase, as there are few broken-off crystals and dendrites. As the solidification process progresses, the frozen thickness of the cooling walls increases continuously, as shown in Fig. 15(e)–(h). Although the liquid flow along the frozen surface was still downward, the magnitudes of the liquid flow velocity became gradually slower and slower. Note that with the solidification process progressing, a lot of broken-off crystals or dendrites added in to the liquid region of the chamber. Therefore, the velocity vector has not totally been that of the liquid; some had been the velocity vector of the broken-off crystals or dendrites. Unlike the hypoeutectic case, in which flow in the middle of the test chamber became gentler and gentler as the solidification process progressed, in the $NH_4Cl$–$H_2O$ solution solidification, the flow pattern became chaotic and complex. These were some of the reasons:

1. With the solidification process progressing, the frozen thickness on cooling walls of the chamber increased gradually; thermal buoyancy became smaller; the effect of solutal buoyancy became evident gradually. Some dendrites or crystals and liquid near the mush zone were rooted out by the solutal buoyancy, as shown in Fig. 15(g), (g-1), (h), and (h-1), into the bulk liquid in the chamber. The bigger crystals and liquid group with their greater momentum were added into the liquid region in the chamber, which, like big stones thrown into the quiet lake, yielded turbulence. Note that the upward flow near the mush zone driven by the solutal buoyancy did indeed exist. Some previous investigations have provided proof [19], but no velocity vector was shown in the obtained velocity vector drawings as the laser light sheet in the test chamber was located in the middle of the chamber. Because there was a thicker mush zone between the light sheet and the front plexiglass plate of the chamber, flow-tracing particles could not be captured by the camera.
2. As the $NH_4Cl$ crystals or dendrites were broken off, they would entrain into the bulk liquid flow. Some of the dendrites were remelted as they were advected into the higher temperature liquid region. The motion of some dendrites was interrupted or merged.
3. During solidification of the $NH_4Cl$–$H_2O$ solution, some broken-off dendrites or crystals collided with each other so that some of them left the plane of the light sheet, that is, actually flowed in three dimensions. The motion of some dendrites was also interrupted or merged.
4. During solidification of the $NH_4Cl$–$H_2O$ solution, sometimes a larger dendrites group rolled downward along the frozen surface like a snowslide and dispersed. These dispersed dendrites, as well as the liquid of flow downward along the mush zone, had greater momentum and velocity, as shown in Fig. 15(g). When they approach the bottom of the chamber, they push and stir the heaped crystals or dendrites, and liquid moves upward again. Fig. 15(g), (g-2), (g-3), and (g-4) show a set of transient flow patterns. The time spacing is 5 s.

Particle image velocimetry appears to be a good tool to measure flow velocity during the solidification of pure water and ammonium chloride solution. However, there were some defects using PIV to measure flow velocity of a binary mixture during the

solidification process. Particle image velocimetry is a measurement technique for obtaining instantaneous whole field velocities. It is based on the equation

$$\text{Speed} = \frac{\text{distance}}{\text{time}}$$

In PIV the property actually measured is the distance traveled by particles in the flow within a known time interval. A CCD camera is used to detect the position of the seeding particles. The obtained images using the CCD camera are divided into rectangular regions called interrogation areas, and for each of these interrogation areas the image from the first and second pulse of the light sheet are correlated to produce an average particle displacement vector. Dividing with the known time between the two images captured, the displacement vectors are converted into a map of so-called raw velocity vectors. Only the average velocity vector can be obtained using PIV, so the details in the mush/liquid interface could not be detected. Because the laser light sheet was located in the middle of the chamber, there was a thicker mush zone between the light sheet and the front plexiglass plate of the chamber. So many uneven tips of dendrites hide from view on the mush/liquid interface that the macrocosm property of these tips of dendrites appears to be a plane. The velocity vectors near the mush/liquid interface appear to parallel the cooling walls. Because of the thicker mush zone between the light sheet and the front plexiglass plate of the chamber, the flow-tracing particles cannot be captured by the camera, so the mush zone cannot be directly identified. This is the major weakness for the application of PIV in the study of the solidification process.

Some of the above velocity vector drawings were asymmetric because the coolant transport pipe system was not perfect so that the cooling strengths of the left and right cooling walls were not the same.

## 4. Conclusion

Particle image velocimetry was used to measure the velocity field during the solidification of water and $NH_4Cl$–$H_2O$ solution. The transient flow field was represented by the vector plots in a consecutive time period. The advantage of this method is its ability to obtain accurate quantitative data. In this study, using pure water solidification, the flow pattern was clearly identified, and the natural convection flow close to the vertical cooling walls was downward at the beginning of the experiment, but gradually changed to an upward flow when the solution began to solidify. Vortex flows formed in the corners of the test chamber. For the $NH_4Cl$–$H_2O$ solution, this type of flow was not seen in the liquid region. Because of the dendrites, there was no clear solid/liquid interface, but a mush region; therefore, the flow was much weaker than in the pure water solidification process. This has been shown in the experiment with the hypoeutectic solution of $NH_4Cl$ and water. It was found that flow is stronger in the beginning of the solidification process, decreasing as it proceeds. The double-diffusive convection patterns for different concentration hypoeutectic $NH_4Cl$–$H_2O$ solution solidification processes were fundamentally the same. Only the freezing speed differed. Changing the cooling strength only changed the freezing speed. The flow pattern of double-diffusive convection of hypereutectic solution of $NH_4Cl$–$H_2O$ has evident difference in comparison with the hypoeutectic solution. It actually is a two-phase flow. The broken-off dendrites or crystals as solid were added into the liquid region of the test solution so that the flow pattern of the total liquid region was very complex and chaotic.

Modeling predictions and comparison with the PIV measurement of the flow field during solidification is designated for future work and is in progress.

## Acknowledgements

The results presented in this paper were obtained in the course of research sponsored by the National Science Foundation. The authors also appreciate the help of Yaozhong Liu in the experimental measurements.

## References

[1] H.E. Huppert, The fluid mechanics of solidification, J. Fluid Mech. 212 (1990) 209–240.
[2] H.E. Huppert, R.S.J. Sparks, Double-diffusive convection due to crystallization in magmas, A. Rev. Earth Planet. Sci. 12 (1984) 11–37.
[3] W.D. Bennon, Numerical simulation of binary solidification in a vertical channel with thermal and solutal mixed convection, Int. J. Heat Mass Transfer 31 (1988) 2147–2160.
[4] C. Beckermann, R. Viskanta, Double-diffusive convection during dendritic solidification of a binary mixture, PCH Physical Chemical Hydrodynamics 10 (1988) 195–213.
[5] M.E. Thompson, J. Szekely, Mathematical and physical modeling of double-diffusive convection of aqueous solutions crystallizing at a vertical wall, J. Fluid Mech. 187 (1988) 409–433.
[6] C.M. Oldenburg, F.J. Spera, Numerical modeling of solidification and convection in a viscous pure binary eutectic system, Int. J. Heat Mass Transfer 34 (1991) 2107–2121.
[7] S. Asai, I. Muchi, Theoretical analysis and model exper-

iments on the formation mechanism of channel-type segregation, Trans. ISIJ 18 (1978) 90–98.
[8] K. Murakami, T. Okamoto, Formation of equiaxed zone in castings, Metal Science 18 (1984) 103–111.
[9] M.S. Christenson, F.P. Incropera, Solidification of an aqueous ammonium chloride solution in a rectangular cavity, Int. J. Heat Mass Transfer 32 (1989) 47–68.
[10] C.S. Magirl, F.P. Incropera, Flow and morphological conditions associated with unidirectional solidification of aqueous ammonium chloride, HTD Vol. 206-1, Topics in Heat Transfer 1 (1992) ASME.
[11] C.F. Chen, F. Chen, Experimental study of directional solidification of aqueous ammonium chloride solution, J. Fluid Mech. 227 (1991) 567–586.
[12] T.D. McCay, M.H. McCay, S.A. Lowry, L.M. Smith, Convective instabilities during directional solidification, J. Thermophysics Heat Transfer 2 (1988) 345–350.
[13] M.H. McCay, T.D. McCay, Optical analyses of fluid flow effects on directional dendritic solidification rates in $NH_4Cl$–$H_2O$ solution, HTD Vol. 234, Heat Transfer in Melting, Solidification, and Crystal Growth, ASME (1993).
[14] J. Dosch, H. Beer, Numerical simulation and holographic visualization of double-diffusive convection in a horizontal concentric annulus, Int. J. Heat Mass Transfer 35 (1992) 1811–1821.
[15] C.F. Chen, D.G. Briggs, R.A. Wirtz, Stability of thermal convection in a salinity gradient due to lateral heating, Int. J. Heat Mass Transfer 14 (1971) 57–65.
[16] H.E. Huppert, P.F. Linden, On heating a stable salinity gradient from below, J. Fluid Mech. 95 (1979) 431–464.
[17] T. Nishimura, M. Fujiwara, N. Horie, H. Miyashita, Temperature visualization by use of liquid crystals of unsteady natural convection during supercooling and freezing of water in an enclosure with lateral cooling, Int. J. Heat Mass Transfer 34 (1991) 2663–2668.
[18] W.Z. Cao, D. Poulikakos, Transient solidification of a binary mixture in an inclined rectangular cavity, J. of Thermophysics Heat Transfer 6 (1992) 326–332.
[19] M.S. Christenson, F.P. Incropera, Solidification of an aqueous ammonium chloride solution in a rectangular cavity-1. Experimental study, Int. J. Heat Mass Transfer 32 (1989) 47–68.
[20] T. Nishimura, T. Imoto, H. Miyahsita, Occurrence and development of double-diffusive convection during solidification of a binary system, Int. J. Heat Mass Transfer 37 (1994) 1455–1464.